Received: 27 May 2020 | Revised: 5 November 2020 | Accepted: 14 December 2020

DOI: 10.1002/we.2609

WILEY

RESEARCH ARTICLE

Machine learnt prediction method for rain erosion damage on wind turbine blades

Alessio Castorrini[1] | Paolo Venturini[2] | Alessandro Corsini[2] | Franco Rispoli[2]

[1]School of Engineering, Università della Basilicata, Potenza, Italy

[2]Department of Mechanical and Aerospace Engineering, Sapienza Università di Roma, Rome, Italy

Correspondence
Alessio Castorrini, School of Engineering, Università della Basilicata, Viale dell'Ateneo Lucano 10, 85100 Potenza, Italy.
Email: alessio.castorrini@unibas.it

Funding information
European Union and the Italian Ministry of Research, Grant/Award Number: Programma Operativo Nazionale Ricerca e Innovazion

Abstract

This paper proposes a paradigm shift in the numerical simulation approach to predict rain erosion damage on wind turbine blades, given the blade geometry, its coating material, and the atmospheric conditions (wind and rain) expected at the installation site. Contrary to what has been done so far, numerical simulations (flow field and particle tracking) are used not to study a specific (wind and rain) operating condition but to build a large database of possible operating conditions of the blade section. A machine learning algorithm, trained on this database, defines a prediction module that gives the feature of the impact pattern over the 2-D section, given the wind and rain flow. The advantage of this approach is that the prediction becomes much faster than using the standard simulations; thus, the study of a large set of variable operating conditions becomes possible. The module, coupled with an erosion model, is used to compute the erosion damage of the blade working on specific installation site. In this way, the variations of the flow conditions due to dynamic effects such as variable wind, wind turbulence, and turbine control can be also considered in the erosion computation. Here, we describe the method, the database creation, and the development of the prediction tool. Then, the method is applied to predict the erosion damage on a blade section of a reference wind turbine, after one year of operation in a rainy onshore site. Results are in good agreement with on field observations, showing the potential of the approach.

KEYWORDS
data-driven methods, machine learning, rain drop erosion, wind turbine blades

1 | INTRODUCTION

During the last decades, wind energy conversion has had a continuously rising trend in terms of global installed capacity (almost 30% in the last three years),[1,2] and wind turbine size.[2–5] For what regards the latter factor, 10-MW offshore wind turbines with a 164-m rotor diameter, were commercially available in 2019. By 2030, it an increase of rotor diameter to more than 230 m in offshore wind farms is expected.[1] Assuming that the rotor diameter is 164 m and the rotor speed is 12 revolutions per minute (typical value for such a wind turbine size), the resulting tip speed is above 100 m/s. This becomes a critical element both for the structural resistance of the blades and for the erosion and damages linked to atmospheric agents. Sandstorms, heavy rainfall, and hailstone can wear the blade coating in a very short period of time. For what regards multi-MW wind turbine blades, the mentioned phenomena play an even more important role: They affect the blade material causing modification of the blade aerodynamics

and degradation of the whole machine performance.[6,7] The drag coefficient of a wind turbine blade may increase more than 200% due to erosion.[8] A deeply eroded leading edge could result in up to 20%–25% annual energy losses as widely demonstrated and reported in the literature (see, for instance, previous studies[8–10]). The erosion severity depends on the operative conditions of the wind turbines. Sierra and Pérez[11] studied the erosion on 201 rotor blades of a 67-MW wind farm. They found that after 14 years of operations, the 87% of the blades had visible signs of erosion, while up to the 50% of them showed a severe level of leading edge erosion. In other works (i.e.,[6,12]), leading edge erosion was found after 2 to 3 years of operations. This means that a wind turbine may start losing its performance very early. In 2016, a big offshore wind farm company had to remove and repair all the 273 blades of one of its wind farms after just 6 years of operations due to severe erosion.[13] Therefore, the investigation of the effects of erosion phenomena on wind turbine blades is gaining momentum in the industrial and scientific community.

The study and prediction of blade damage and its effect on the turbine performance has been a fertile terrain for developing new theories, models, and experiments. Zhang et al.[14] experimentally studied the erosion of wind turbine blade coatings using discrete water jets by analyzing the effect of the presence of a liquid film on the blade surface and of the surface curvature. Amirzadeh et al.[15,16] published an interesting two parts work on a computational tool for analyzing rain erosion in wind turbine blades. In Part I, the scholars present a stochastic raindrop model and a simulation of its impact on solid objects, while, in Part II, they imported into a finite element model of the blade shell the predicted impact pressure profiles in order to study the related stresses within the blade coating and to evaluate the fatigue damage accumulation rates. All these results are then used to estimate the expected fatigue life of the blade coating in terms of incubation period. In Slot et al.,[17] it is offered a review of the models that have been developed to estimate the coating life under rain erosion conditions is presented. Eisenberg et al.[18] developed an analytical surface fatigue model to estimate the initiation of leading edge erosion on wind turbine blade coatings due to rainfall. Li et al.[19] have developed a numerical simulation to investigate the effect of the wind speed, droplet size, and density on the erosion of wind turbine airfoils. A further experimental and simulation work has been offered by Maniaci et al.[20] Here, the authors have first measured the surface roughness and erosion pattern of several wind turbine blades, then they statistically reproduced these patterns on representative tip and mid-span blade strips in wind tunnel tests. Furthermore, they developed a computational model to reproduce the experiment. Results from the computational fluid dynamics (CFD) model developed in Hossam El-Din et al.[21] are, firstly, coupled to the blade element momentum (BEM) theory and then applied to estimate annual energy production loss for a wind turbine operating in the Saharan environment. Finally, Fiore et al.[22–24] focused the attention on modeling and simulating solid particle erosion of wind turbine blades.

During the last decade, we started to develop and to implement a large set of models and techniques to simulate particle/droplet erosion and deposition processes on turbomachinery blades. In previous studies,[25–28] for instance, we modeled and studied the particle deposition process in turbine and compressor blades and cooling passages, with and without the effect of temperature. Papers[29–32] were focused on modeling of solid particle erosion: In these papers, we studied the erosion phenomenon in relation to sand or coal fly ash, paying particular attention to blades of industrial fans. In 2015, we presented an approach to evaluate the severity of rain erosion damage in multi-MW wind turbine based on the water hammer pressure exerted during a droplet impact.[33] In Castorrini et al.,[34] we computed the distribution of rain erosion damage thickness on a wind turbine blade, adopting the particle cloud tracking[34–36] model and solving the flow field with the Reynolds-averaged Navier–Stokes (RANS) approach. In Castorrini et al.,[36] we developed a new algorithm to perform CFD simulations of long-time erosion process accounting for the shape modification of the blade. In that work, the introduction of some appropriate scale factors and erosion threshold limits for geometry modification allowed us to simulate years of operating conditions. By adopting the same technique, in Castorrini et al.,[37] we simulated the time evolution of the erosion process on the blade of an induced draft fan. In Castorrini et al.,[38] we analyzed performance deterioration of a wind turbine strip subjected to rain erosion by adopting the particle cloud tracking model. A similar approach was used in Castorrini et al.[39] together with the solid-extension mesh moving technique[40] in order to take account of the geometry (mesh) modification while the erosion is progressing. The long-time evolution process predictive algorithm was then extended to study particle deposition on the blade of an axial fun used in tunnel ventilation.[41] The same algorithm developed and tuned in the previous publication was finally experimentally validated studying the erosion of an aluminum–alloy specimen exposed to sand-laden flow.[42] In the present paper, we focus our attention on rain erosion of wind turbine blades; yet the proposed approach can be easily extended to other applications.

Independently from the models developed, the approach adopted so far strongly links the simulations of the considered blade to specific operating conditions. This neglects the stochastic variability of the wind and rain in real life, which occur both because the turbines are installed in different places and because the conditions are not constant over time. Furthermore, from an industry point of view, it would be very beneficial having a tool capable of predicting the behavior of a blade in real conditions. In the current approach, this could be done by performing many simulations of the different operating conditions to which a machine can be subjected. Alternatively, an unsteady simulation can be performed. Both these solutions are unfeasible because they require prohibitive computational times, and, anyway, they would predict the behavior of a wind turbine only in a specific installation site. It is therefore necessary to make an effort to change the simulation approach, passing from the current case-specific one, to an innovative one, more flexible and capable of predicting quickly the behavior of a given wind turbine (or blade profile) under the different operating conditions it may encounter in the environment it is installed.

The capability of prediction of the erosion of wind turbines under real conditions would contribute to take account of the loss of performance in wind farms and of the risk of blade failure. This would turn maintenance routines from being preventive into being predictive. With the support of predictive tools, we can estimate when a wind turbine operating under certain conditions reaches a performance level below which it is

recommended to perform maintenance; in this way, the maintenance scheduling moves from a statistical (preventive) to a real operating condition based (predictive) approach. For this reason, such predictive tools must be fast, reliable, and easy to use.

The aim of this study is to define a computer application able to predict the erosion damage on blade sections managing the full spectrum of wind turbine operation and rain conditions. In doing so, we capitalize the experience developed on the numerical simulation of rain erosion, extending the applicability of the methods to take account of the dynamic variation of the operating condition of the wind turbine blade. The proposed tool couples the numerical simulation of fluid and droplet dynamics with a tailored machine-learning algorithm.

The whole picture of the prediction tool here proposed is shown in Figure 1. The idea is that for a given blade section, operation period, and environmental conditions, the aerodynamic field and the particle flow relative to the section are taken as input. Such quantities can derive from either field measurements or simulations and are inputs for the present tool. Given these inputs, a machine learnt predictor trained on a database of all the possible operating conditions for the selected blade is applied to predict the impact pattern of the droplets on the blade profile. Such impact pattern is then elaborated by the erosion and scale-up models. This provides us as final result the erosion damage distribution for the given environmental conditions on the considered blade section.

In the present paper, we first describe the models used to build up the whole tool, and, secondly, we apply them to predict the erosion on a reference blade section.

More specifically, numerical simulations are used to build a database of 2-D cases in which the droplet dynamic is resolved for a large set of possible section relative flow conditions and rain droplet sizes. The machine learning (ML) module is then trained on this database to be allowed to predict a droplets impact pattern on the section surface at any given operative condition. This is the focus of Sections 2 and 3. The one-way coupling approach can be adopted in the case of simulation of rain droplets dynamics (see previous studies[33,34,43,44] and Section 2.1). This approach allows us to use the steady 2-D aerodynamic field as base for the particle tracking simulation. Furthermore, working with 2-D sections permits us to drastically reduce the computational cost in the database generation, but it also allows the tool to work together with multibody and dynamic wind turbine simulators (e.g., based on the BEM theory). The strength of this idea resides in the fact that we can retain the accuracy of advanced numerical simulation for droplet dynamics taking account of the input given by a dynamic simulation of the entire machine in operation under turbulent wind inflow.

The next step involves the use of the impact pattern to estimate the erosion damage on the blade section. A rain erosion model will be then used in couple with a scale-up procedure to project the results to real field data. These parts are described in Section 4. Section 5 presents the application of the tool developed to predict the erosion damage on a specific wind turbine blade section. For this application, the erosion damage is computed in dynamic conditions (with turbulent wind inflow defined by the IEC standard) and taking account of all the possible wind velocities encountered by an outboard blade section of a 5-MW horizontal axis wind turbine during a year of normal operation in a rainy site.

We want to underline that the individual components of the tool have been validated in the past by the authors (i.e., flow field solution and particle tracking) or by other researchers (i.e., the erosion model). The machine learnt prediction tool developed for the present work is validated with the simulations performed beside those used for building the database, as shown in Section 3.5. On the contrary, there are not available specific data to directly validate the sample application (5-MW horizontal axis wind turbine), so the comparison with the real field observations could be only qualitative (Section 5).

2 | RAIN DROPLET IMPACT PREDICTION TOOL, METHODOLOGY

First, we define the rationale of the prediction tool developed to simulate the impact pattern of rain droplets on airfoils for a given wind turbine section in any expected state of operation and rain. Figure 2 gives a schematic overview of the process of definition of the prediction tool.

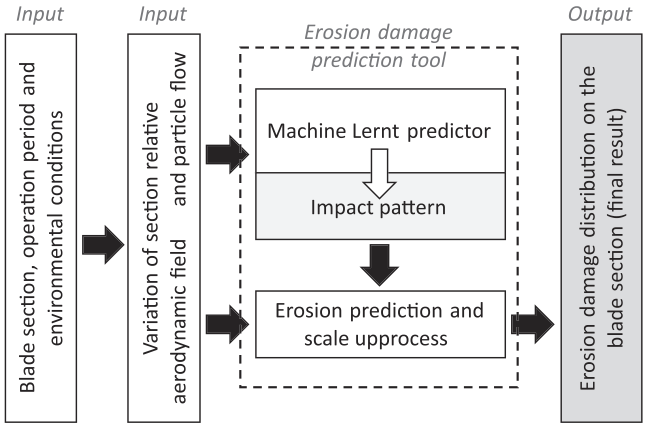

FIGURE 1 Flow diagram of the whole erosion damage prediction process

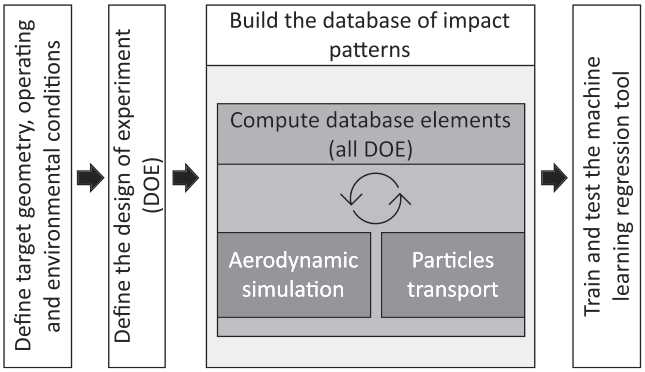

FIGURE 2 Prediction tool for droplet impact pattern, flow diagram

Starting with a wind turbine blade section and an expected range of operating and environmental conditions, it is possible to derive a plausible design of experiment (DOE) for the conditions (relative flow and rain) in which this section is expected to work. For each of these conditions, we evaluate the expected impact pattern of the droplets over the airfoil section using a pipeline of in-house developed multiphase flow solvers. In this way, we build a database of flow and particle (droplet) properties spreading over all the possible conditions and including rain and impact pattern over the airfoil line. Finally, we turn the discrete dataset into a regressor able to unveil the correlation among flow and particle dynamics using a ML method based and trained on the multivariate dataset.

The prediction of particle laden flows requires a multiphase and multi-physics modeling ecosystem. Accordingly, each element of the database is obtained by coupling a set of dedicated numerical tools and procedures.[33,36,38,39] In order to simulate the particle transport in the airflow, we adopt the strategy used in our previous works: A steady turbulent flow simulation for the relative wind at the section provides the velocity and turbulent field necessary for the particle tracking simulation (see previous studies[33,36,38,39] and Section 2.1). This simulation is repeated for a wide range of relative inflows and particle characteristics to spread the expected operating conditions of the selected turbine blade section. All the data obtained from these simulations are then processed to create a database we use to train the ML regression tool.

More specifically, we have purposely created a training dataset by inferring the set of independent input features from the open literature and by using an ad hoc chain of simulations to compute them.

The features selected for the training data set describe the ensuing phenomena:

- Relative wind aerodynamics (Reynolds number and angle of attack)
- Particle-surface impacts (number, velocity, and angle)
- Particles characteristics (size, material, and concentration).

For the sake of generalization, each of these quantities is considered per unit of time and characteristic length of the problem (typically, the blade span).

In surveying the available open literature on erosion models commonly used in numerical simulations, we noticed that the common output is the *erosion rate* on target material. Most of the correlations and models (see, for instance, previous studies[45–47]) understand this quantity as dependent upon (i) particle kinematics impacting the surface (velocity and direction), (ii) particle inertia and concentration in the flow, and (iii) surface material. An essential difference can be found in the case of liquid particles, where the erosion damage is also correlated to the so-called incubation period.[48] The understanding of the incubation period presupposes the history of the impacts on the surface. This aspect must be considered in the definition of a prediction tool that can be used for a generic operating condition of the wind turbine. Indeed, it is not possible to directly scale the erosion damage or the erosion rate if an incubation period is considered in the erosion model.[39] However, we showed in Castorrini et al.[39] that the number of impacts is linearly scalable using the ratio between simulated and real particle flow. Therefore, in previous studies[49,50] and here, we introduce the incubation energy (as function of the latter two quantities) in order to scale the computed impact data with a real operating condition or time period (see Section 4 for details). This choice allows us to apply the erosion model in post-processing, after having scaled the impact pattern and having assumed as outputs of the regressor the impact velocity (V) normalized by the freestream relative velocity, the impact angle (θ), and the impact count per unit surface (n_p). The impact angle is defined here as the angle between the impact velocity and the surface tangent plane in the impact location.

Impact characteristics are generally defined as function of the position on the airfoil line; furthermore, they are implicit variable of the particle dynamic problem. Therefore, we need to find a set of input features that identify each specific impact. Particle transport characteristics are related to the flow field and to the inertial and geometrical characteristics of the particles.

The relative wind aerodynamics and particle characteristics are inputs of the two-phase flow simulation; accordingly, we add them into the set of input features for the database element, while we can consider the impact characteristics as the output of the regressor (i.e., of the generic database element).

Through a set of these features, one can identify the generic element of the database by the following relation.

$$\begin{Bmatrix} V \\ \theta \\ n_p \end{Bmatrix} = \mathfrak{I}(\xi_G, \xi_F, \xi_P), \tag{1}$$

where ξ_G represents a feature describing the geometry of the target, ξ_F represents a feature describing the relative flow velocity, and ξ_P represents a feature describing geometry of the particles.

In Equation (1), we do not consider the implicit dependency on the particle concentration (C) because the particle concentration affects the impact count linearly; as a consequence, its effect can be applied in post-processing through a proper scale factor (see Section 4).

Equation (1) gives the normalized impact situation over the airfoil boundary for a particular condition of the particle laden flow.

2.1 | Computational fluid–particle dynamics

To evaluate V, θ, and n_p for each database element (section relative flow ξ_F and rain condition ξ_P), we first solve the steady aerodynamic field for the given condition, and we then use this field to drive the rain droplet motion in a particle tracking simulation.

The flow field solutions have been obtained by performing the steady state CFD simulation of the blade strip. The blade strip is cylindrical, so no variation of chord length or twist is applied, and the flow field is constant along the blade span. This assumption allows to degenerate the domain volume for the CFD and to run a 2-D aerodynamic simulation.

OpenFOAM v1806 have been used for all the fluid phase computations. The CFD solver adopted is the Semi Implicit Method for Pressure Linked Equations (SIMPLE), applied to solve the RANS equations for an incompressible fluid. The standard k–ε turbulence closure model has been adopted for all the computations. Wall functions are used to model the wall boundary layer.*

In the particle tracking simulations, the domain is defined over the 3-D blade strip. Accordingly, the aerodynamic field obtained in the CFD simulation is symmetrically extended over the finite spanwise extrusion of the blade strip domain. This choice allows to have more erosion data to be averaged on the blade span length and thus to obtain a more relevant statistical result.

Droplet dynamics is modeled in a Lagrangian frame by using a one-way coupling approach. This approach is proven to be accurate under the hypothesis of small droplet volume fraction[43,44]. This means that the droplet motion is governed by the flow field but the flow field is not affected by the droplets.

Droplet motion is computed by solving the Bassett–Boussinesq–Oseen (BBO) equation expressing the conservation of momentum for the particle phase. According to Armenio and Fiorotto,[51] only the drag force makes a not negligible contribution to the droplet dynamics; thus, only the aerodynamic drag is considered in the droplet equation of motion. The effect of turbulent dispersion of droplets is taken into account by adopting the stochastic eddy lifetime method, also known as the discrete random walk (DRW) model. DRW model decomposes droplet velocity into an average term $\bar{\boldsymbol{u}}$ and a fluctuating one $\acute{\boldsymbol{u}}$. The former is computed by solving the BBO equation and by considering the RANS solution of the flow field. The fluctuating term is evaluated as described in[52]

$$\acute{\boldsymbol{u}} = \sigma\boldsymbol{\zeta} \tag{2}$$

ζ being a vector of normally distributed random numbers, $\sigma = \sqrt{2k/3}$, and k is the turbulent kinetic energy computed by the RANS solution. In Greifzu et al.,[52] the DRW model demonstrated a very good agreement with experimental data; therefore, it is considered reliable and adopted in the present paper.

2.2 | ML algorithm

The machine learnt predictor is designed to solve a regression problem and provide a representation of function $\mathfrak{I}$ of Equation (1). Given the position along the airfoil line, the inflow relative wind, and particles size, the algorithm should be able to predict the expected value of the particle impact features in the location (V, θ, n_p).

*It must be notified that the use of a wall functions approach produces not accurate results for high angles of attack. For the application presented in this paper, we decided to accept this approximation, to limit the computational cost of the database generation. Furthermore, we notice that the selected section of the wind turbine blade in normal operation works at low angle of attack for most of the samples considered (see Figure 13).

Starting with the database of cases created by solving Equation (1) by numerical simulations, the algorithm is then trained to predict the output features separately. This means that the training is repeated for each output feature, and three different regressors are defined at the end of the training step.

The single regression problem is solved applying the extreme GBoost (or XGBoost) algorithm.[53–55] XGBoost is an implementation of gradient boosted (GBoost) decision trees[56] designed for improving speed and performance. XGBoost is an open source package available at https://github.com/dmlc/xgboost,[57] and it is used for supervised learning problems. The gradient boosting leaner determines a prediction in the form of an ensemble of simpler learners (i.e., decision trees). It creates each learner sequentially allowing the new developed predictor to learn from the errors committed by the previous ones. The present study uses an efficient implementation of XGBoost with multithread parallelization, sparse data awareness, and cache access. The optimal tuning of iper-parameters has been done using a random search.[58]

3 | RAIN DROPLET IMPACT PREDICTION TOOL, COMPUTATIONS

3.1 | Definition of the DOE

A large training database was created by adopting the automatic interface described below. The aim is to produce a large number of CFD simulations coupled with the particle tracking computations in a wide range of operative conditions, by varying the far field wind speed, the angle of attack, and the droplet size.

Each element of the database is obtained by using the automatic interface described by the algorithm in Figure 3; the figure also shows the sections of the present work in which the various parts of the algorithm are described in detail.

Notably, the algorithm can be easily generalized to any kind of aerodynamic condition, particle laden flow, and erosion regime to create an erosion damage model correlated to the position along the surface of the blade. The creation of the training dataset can also be complemented with the inclusion of experimental subsets (if available).

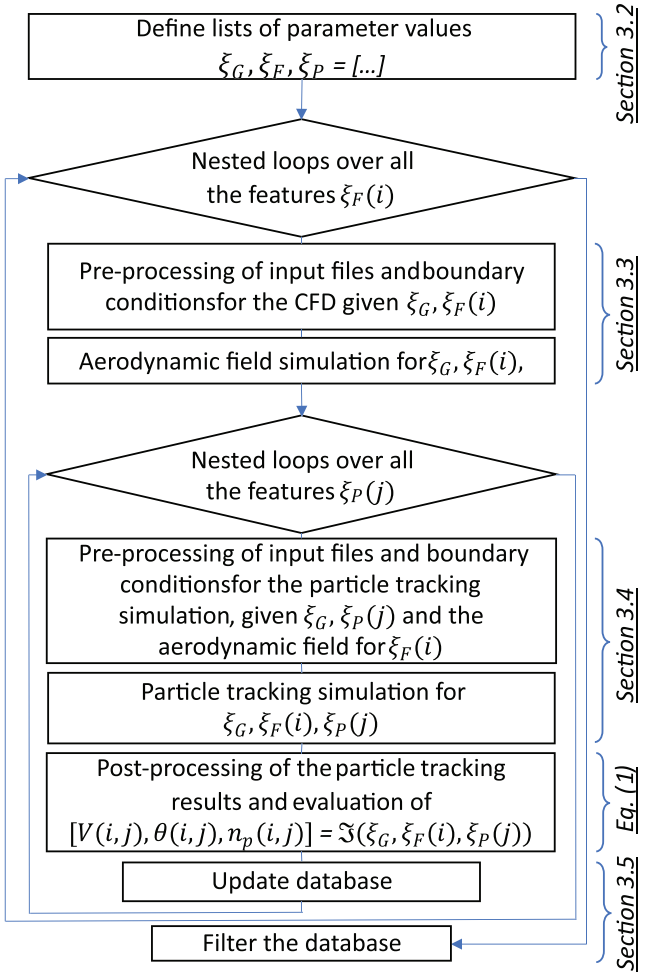

FIGURE 3 Database generation algorithm

As this study is in its first stage, it is emphasized that an extension of the features related to the airfoil geometry would make the final database suitable for more general purposes.

Following the generic methodology exposed in Section 2, we define here (Table 1, columns 1–3) the database features and their value bounds for the specific application. We consider the section relative Reynolds number and the angle of attack as input features for the group ξ_F, to characterize the aerodynamic condition at the section. The Reynolds number is a suitable nondimensional number that contains both the information about the geometry and the inflow relative velocity.

To characterize the airfoil shape, we select as feature for the group ξ_G, the airfoil coordinate defined by the curvilinear abscissa running over the airfoil shape line. The airfoil coordinate s starts and ends at the trailing edge of the airfoil, going from the suction side to the pressure side, and it is normalized with respect to its maximum value. Finally, we select the particle diameter per unit chord (d_p) of the airfoil as feature of the particle size ξ_P.

Table 1 reports also the DOE bounds and number of sampling values used for each feature. Each combination of these parameters represents an element of the database generated iteratively with the algorithm of Figure 1. The final number of database entries is therefore 1.94×10^5, corresponding to 56 aerodynamic simulations and 432 particle tracking simulations.

3.2 | Reference wind turbine section

The method described in the previous sections is applied to the airfoil used on the outboard region of the 5-MW reference blade defined by the National Renewable Energy Laboratory (NREL) and reported in Jonkman et al.[59] The blade design assumes a NACA64618 from the 70% of the span up to the tip region; accordingly, in the present work, this is assumed as the base section for all the simulations. As first approximation, we can expect the section to work for normal operation in a range of Reynolds number from 7×10^5 to 1.4×10^7 and in a range of angle of attack going from -10° to 20°. These values are selected in view of the final application, where the unsteady aerodynamics of the rotor is considered for an entire range of operating conditions under turbulent inflow. The range of Reynolds numbers is mostly related to the variable rotor speed, the variability of the chord along the span defined by the same airfoil, and the variability of the wind velocity. The range of angles of attack must be analyzed considering the variation connected to the turbulent wind inflow and to the action of the pitch control. Moreover, we have to specify a size range for the particles. Because in this work we are simulating rain erosion, we are interested to particle size ranging between 10 μm and 2 mm. The feature ranges, and the number of samples for each feature are summed up in Table 1 (right side, columns 4 and 5). Yet the working range can be easily extended or reduced.

3.3 | Aerodynamic simulation details

The aerodynamic simulation is performed to predict the turbulent flow field needed to compute the particle motion around the reference size section (unit chord airfoil). Therefore, all the simulations are performed on a generic grid of the normalized airfoil, varying the flow direction and Reynolds number at the freestream inlet. Figure 4 shows the grid, which is a 3-D unstructured mesh, made by extruding one layer of a 2-D grid composed of two blocks (Figure 4, left). The external block is a quadrilateral unstructured domain of 6000 cells, with all sides 40c (c is the chord length) far from the airfoil. The internal block is a structured O-shaped grid of 10c radius composed of 50,000 elements. The O-grid is obtained by hyperbolic normal extrusion with a 1.2 growth rate at the wall and a wall distance of $1.0 \times 10^{-5}c$ to ensure y^+ less than 100 for all the Reynolds configurations studied. We used 386 elements to describe the airfoil shape to have a good resolution in the impact computation on the surface (Figure 4, center). The domain is then defined in a nondimensional frame of reference, which has the origin at the leading edge of the blade section, X axis oriented from the leading edge to the trailing edge and Y axis to define the right hand frame.

The domain counts one cell in the direction normal to the airfoil; therefore, it can be treated as 2-D grid by the aerodynamic solver. The boundary conditions imposed in the simulations are

TABLE 1 Features selection and DOE definition

Feature group	Selection	Symbol	Value	Samples
ξ_G	Airfoil coordinates	s	$0 \div 1$	386
ξ_F	Angle of attack	α	$-10^\circ \div 20^\circ$	7
ξ_F	Relative flow Reynolds number	Re	$7 \times 10^5 \div 1.4 \times 10^7$	8
ξ_P	Particle diameter per unit chord (nondimensional particle diameter)	d_p	$10 \times 10^{-6} \div 2000 \times 10^{-6}$	9

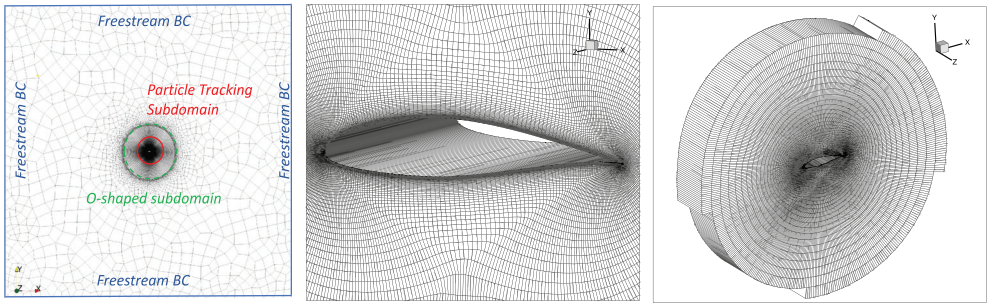

FIGURE 4 Simulation mesh: whole mesh (left), blade zoom (center), and mesh zone for particle tracking simulation (right)

- no-slip condition for the velocity at the blade wall
- freestream fixed value inlet for velocity and turbulence quantities
- zero-gradient condition for the pressure and for all the variables at the outflow surface
- As an example of results of the CFD simulation, Figure 5 shows the pressure field and the streamlines for $Re = 2.5 \times 10^6$ and $\alpha = 10^\circ$.

3.4 | Particle tracking simulation details

To avoid excessive computational cost in generating the database, the particle tracking simulations are performed using a sub-zone of the aerodynamic mesh (Figure 4, right). The flow field outside this zone (upstream the blade) is scarcely affected by the blade, so we can assume that particle dynamics does not change in the far field region. The sub-grid (Figure 6) is extracted as a cylindrical region with axis passing through the center of the airfoil and parallel to the Z axis, with a radius of 3c.

The number of injection cells and simulated particles is chosen in order to guarantee the full covering of the airfoil surface and to ensure statistically relevant results in terms of impacts. This is an important aspect because in the post-process scaling up procedure of the damage it is crucial to have a statistically relevant number of impacts to avoid an unreliable prediction. This effect is achieved by injecting at the initial simulation time 200 particles per injection cell. The injection cells are selected automatically for each angle of attack as reported in Figure 6. We define the injection cell set as the intersection between the mesh and two arcs drawn on a plane orthogonal to the Z axis. The origin of the arcs is the center of the airfoil, the radius length equals 3c, and the $\pm\gamma$ angle is measured from the line directed as the inflow velocity and passing through the airfoil center. The span of γ is the same for all the simulations, and it is taken large enough to have a particle beam completely containing the airfoil shape area (see Figure 5, right). For the range of angles of attack considered in the database, we found $\gamma = 30^\circ$ to be a reasonable choice.

Figure 7 shows an example of the particle tracking simulation (PTS) results, for the same sample point at $Re = 2.5 \times 10^6$, $\alpha = 10^\circ$, and with a nondimensional particle diameter $d_p = 50 \times 10^{-6}$.

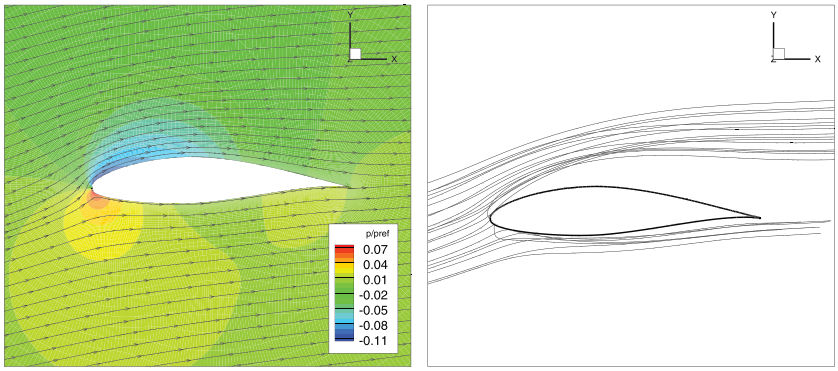

FIGURE 5 Pressure field and streamlines (left) and particles trajectories (right)

FIGURE 6 O-shaped mesh and droplet inflow region

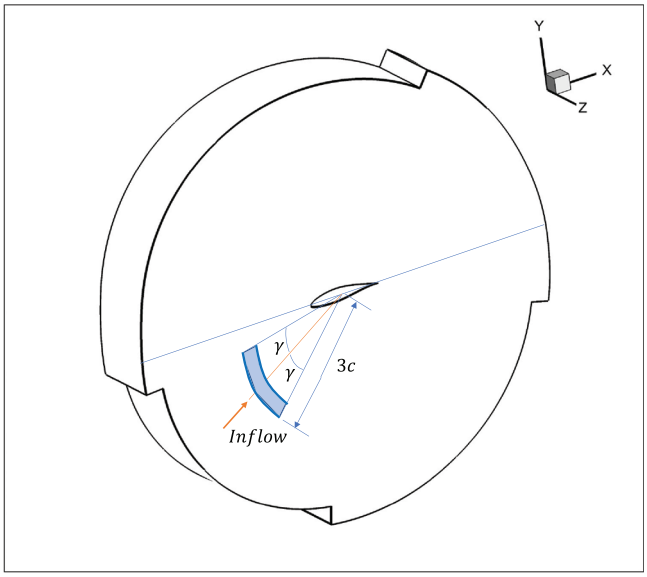

FIGURE 7 Results example: normalized impact count (top), impact velocity (center), and impact angle (bottom). $Re = 2.5 \times 10^6$, $\alpha = 10^\circ$, nondimensional particle diameter $d_p = 50 \times 10^{-6}$

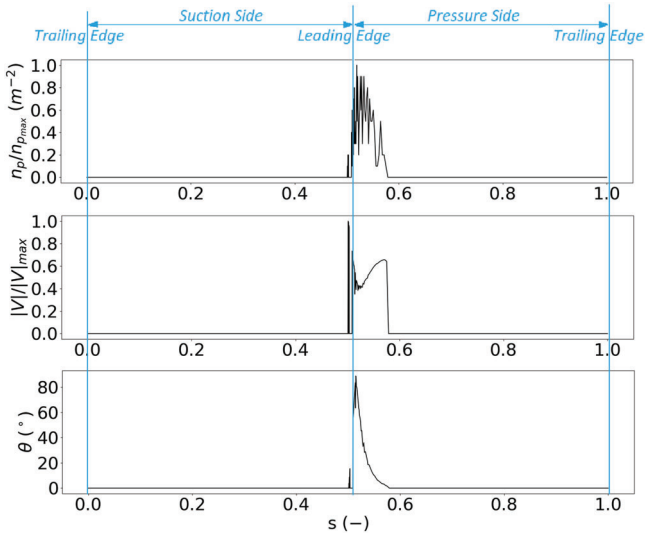

3.5 | Final database and ML

The whole parallel computation for the database takes around 72 h on 8-core 2.3 GHz machine. The analysis of the data obtained gives already the possibility to extract some general considerations about the behavior of the solution in terms of impact distribution and characteristics over the airfoil surface and on its dependency on the various input variables. Some sample results are reported in Figure 8.

Figure 8 (left) shows the variation of the impacts count per unit surface over the curvilinear abscissa by varying the angle of attack for a sample nondimensional particle diameter of $d_p = 50 \times 10^{-6}$, at $Re = 12.5 \times 10^6$. As expected, the maximum is predicted on the leading edge for small angles of attack. The peak moves from the suction side to the pressure side by increasing the angle of attack. The reason for this behavior is shown in Figure 9. Increasing the angle of attack results in a modification of the region of the blade profile exposed to droplets impacts (yellow lines in figure). In particular, the region in the suction side decreases and that in the pressure side increases, Therefore, the peak in the number of impacts shifts accordingly.

Figure 8 (right) reports the variation of the impacts count over the curvilinear abscissa at an angle of attack $\alpha = 5^\circ$ by varying the particle diameters at $Re = 12.5 \times 10^6$. It is noted that the impact pattern shows an M-shaped maximum around the leading edge, with the two peaks spacing out as the droplet size increases. This is clearly related to the particle inertia: At the leading edge, the flow deviation is strong, and hence, even relatively large droplets are deviated. This results in a smaller number of impacts at the leading edge and in larger number at its sides, with a more or less symmetric distribution depending on the angle of attack.

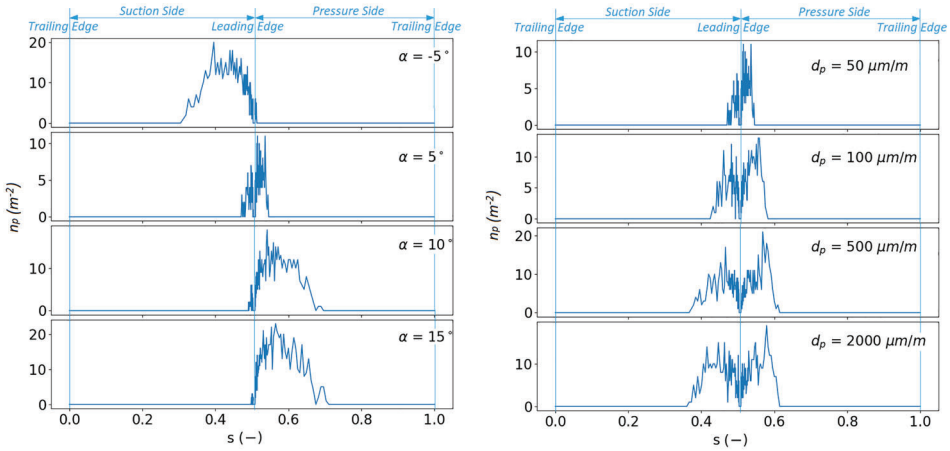

FIGURE 8 Database elements for $Re = 12.5 \times 10^6$, plot. *Y* axis: impact count per unit surface; *X* axis: airfoil coordinate. Left column: plots for fixed $d_p = 50 \times 10^{-6}$ and $\alpha = (-5,5,10,15)^\circ$ (from top to bottom). Right column: plots for fixed $\alpha = 5^\circ$, and $d_p = (50,100,500,2000) \times 10^{-6}$ (from top to bottom)

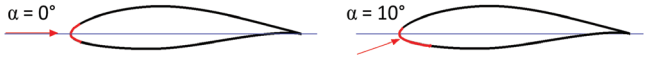

FIGURE 9 Example of variation of the airfoil regions exposed to droplet impacts for two different angles of attack

About 80% of the built database is used to train the ML algorithm, while the remnant 20% is left for testing it. To ensure that the final regression algorithm is able to generalize, and, therefore, to avoid the possibility of overfitting, we performed a fivefold cross-validation. Accordingly, the training is repeated five times with five different configurations of the training–testing dataset, keeping the same proportion. Table 2 reports the results of the fivefold cross validation in terms of coefficient of determination (R^2) for each output.

Table 3 reports the R^2 score of the regression and the MSE (mean squared error). The values reported after testing and cross-validating the regressor show that the ML prediction is sufficiently accurate, as demonstrated also by the plots in Figure 10, which reports the comparison of simulations (blue) and ML (red) in a couple of forwarding tests.

4 | RAIN EROSION MODEL AND SCALE UP PROCEDURE

The rain impact pattern predicted by the regressor described in the previous sections needs some further manipulations to become the erosion damage (viz., thickness) pattern on the given blade section and for a given wind and rain condition. More specifically, we first must apply an erosion model to convert the impacts into erosion, and then we have to scale up the erosion to obtain the real field erosion damage.

Recalling the scheme of Figure 1, in order to compute and scale the cumulative erosion damage, we assume to have a statistically meaningful set of relative wind and rain flow condition experienced by the section during the operating period. In this work, the blade section aerodynamics is taken from a set of dynamic simulations of the wind turbine, in operation under a turbulent inflow wind defined by an average velocity V_{ref}. The

TABLE 2 R^2 score of the regression for the fivefold cross validation

Output	R^2
n_p	[0.9080, 0.9135, 0.9165, 0.9106, 0.9102]
V	[0.9405, 0.9304, 0.9312, 0.9318, 0.9309]
α	[0.9602, 0.9424, 0.9464, 0.9563, 0.9519]

TABLE 3 Accuracy of the regression after testing

Output	R^2	MSE
n_p	0.9143	0.0011
V	0.9385	0.0102
α	0.9560	0.0020

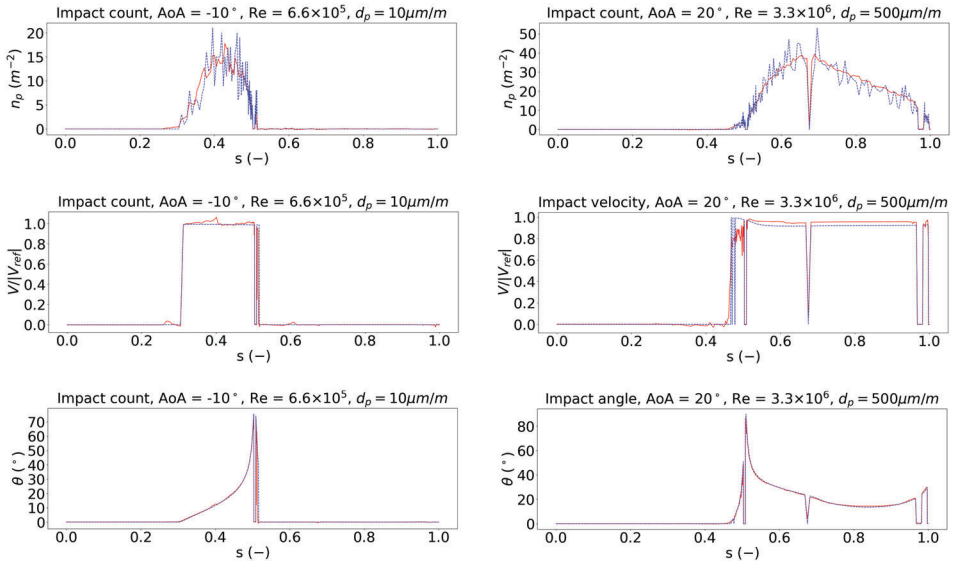

FIGURE 10 ML test, comparison between ML prediction and simulated data (ML prediction in red, simulated in blue). (left) AoA = −10°, $Re = 6.6 \times 10^5$, $d_p = 10 \times 10^{-6}$; (right) AoA = 20°, $Re = 3.3 \times 10^6$, $d_p = 500 \times 10^{-6}$

set of reference velocities is taken by spanning the power curve of the wind turbine. We use the FAST (Fatigue, Aerodynamics, Structures, and Turbulence) code,[60] a multibody and aeroelastic simulator of two- and three-bladed horizontal-axis wind turbines (HAWT) to generate the set of relative flow condition for the given wind turbine blade section.

To consider the site anemometry, the Weibull wind probability density function is used to extrapolate over a year's time. Accordingly, given an installation site and its anemometric data, we can obtain in a very short time a prediction of the possible damage by rain erosion in a given period of time.

We base the calculation of the scaled erosion damage on the modeling adopted in Castorrini et al.[39] We kept the same nomenclature but introducing some modifications.

Here we adopt the model developed by Springer et al.[48] for rain erosion of coating materials, introducing some developments to take account of the variability of the droplets flow and size. This model is based on the observation that erosion, due to a given droplet size impinging the target surface with a given velocity, starts after a threshold impact count $(n_p)_{thr}$ with an approximately linear erosion rate, given by the formula

$$E = a_4 \frac{1}{\left[A_{pp}(n_p)_{thr}\right]^{a5}}, \tag{3}$$

where a_4,a_5 are empirical model constants. The incubation count per unit surface $(n_p)_{thr}$ is computed, according to Springer et al., by the empirical correlation:

$$A_{pp}(n_p)_{thr} = a_1 \left(\frac{S_{eff}}{\bar{\sigma_0}}\right)^{a_2}, \tag{4}$$

where A_{pp} is the projected area of the particle, S_{eff} is a parameter that characterizes the strength of the coating material, $\bar{\sigma_0}$ is the stress produced by the impinging droplet, and a_1 and a_2 are model constants (see Springer et al.[48] for further details). This model is here adopted for predicting the erosion.

In Equation (4), S_{eff} is a constant parameter depending on the target material. All the other quantities are function of the droplets size and impact conditions (impact angle and velocity of the impinging droplet). In Castorrini et al.,[39] we used this model to evaluate the incubation of the damage. In that case, we assumed a unique average condition of fluid and rain flows, but in a more general case, the impact conditions change at every instant (or time step). Therefore, we introduce here the concept of incubation energy $(\Theta)_{thr}$ to bypass the issues related to the variability of $(n_p)_{thr}$ in time.

We start with the expression of the impact energy for a particle impacting the surface in the point s:

$$\Theta = \frac{1}{2} m_p v_{i,n,s}^2, \tag{5}$$

where $v_{i,n,s}$ is the normal component of the particle impact velocity and m_p is the particle mass. The incubation energy associated to the point s of the surface boundary, for a given aerodynamic and particle flow condition (i.e., the one identified by the ith time step of the FAST simulation), is defined as

$$(\Theta)_{\text{thr}} = \frac{1}{2} m_p v_{i,n,s}^2 \, (n_p)_{thr}. \tag{6}$$

Notice that $(\Theta)_{\text{thr}}$ assumes a different value by varying the velocity $V_{ref} = \hat{V}$ and the actual time step $i = \hat{i}$.

We can now assume that the erosion at point s starts when the accumulated impact energy $(\Theta)_{\text{TOT}}$ is greater than $(\Theta)_{\text{thr}}$, at $V_{ref} = \hat{V}$ and $i = \hat{i}$, where

$$(\Theta)_{\text{TOT}} = \sum_{V_{ref} = V_{cut-in}}^{\hat{V}} \sum_{i=1}^{\hat{i}} \Theta^{(V_{ref},i)} F_{ACT} \Delta n_p^{(V_{ref},i)} \tag{7}$$

Here, $\Delta n_p^{(V_{ref},i)}$ is the number of droplet impacting the surface in the time step i of the simulation for the reference velocity V_{ref}, and F_{ACT} is the scale factor per time step, defined in the next paragraph.

It should be emphasized that the number of simulated droplets has been chosen to obtain statistical relevant results, but it is arbitrary. In general, the real field droplet concentration is different from the simulated one, and it also varies in time. Furthermore, also the simulation time is chosen arbitrarily, and thus, we have to scale the result for a given period of operation of the turbine. Therefore, we define the following scale factor:

$$F_{ACT} = \frac{n_R}{n_{TOT}} \frac{T_R f(\text{V}_{\text{ref}})}{\text{T}_{\text{SIM}}} \frac{1}{N_{t\ steps}}. \tag{8}$$

Here, $f(\text{V}) = \left(\frac{k}{c}\right)\left(\frac{\text{V}}{c}\right)^{k-1} e^{-\left(\frac{\text{V}}{c}\right)^k}$ is the Weibull probability density function, $N_{t\ steps}$ and T_{SIM} are the number of FAST simulation time steps and total simulation time respectively, T_R is the operation period (1 year), and n_{TOT} is the number of particles per unit surface injected in the particle tracking simulation. In Equation (8), n_R represents the total number of particles per unit surface, expected to enter the particle tracking simulation domain during the operation time, at the average wind velocity V_{ref}. This is given by

$$n_R = \frac{\text{H}_{\text{BRF}}}{\text{V}_{\text{d}}}, \tag{9}$$

where V_{d}, is the droplet volume and H_{BRF} is defined as in Castorriniet al.[39]

$$\text{H}_{\text{BRF}} = \frac{\text{V}_b}{V_r} \text{H}_{\text{RF}}, \tag{10}$$

where H_{RF} is the amount (in m) of rainfall per unit time, V_{b} is the blade section velocity, and V_r is the raindrop velocity.

Given the particle mass m_p and the density of the target material ρ_t, the erosion damage, expressed as normal displacement of the target boundary due to the material removed by Δn_p impacting particles per unit area in a given time step Δt, reads

$$\Delta e = \frac{E \Delta n_p m_p}{\rho_t} \tag{11}$$

The computed erosion Δe represents the thickness of the eroded material along the blade section due to the simulated rain droplets. The scaled erosion displacement for each time step e_{SU} can be written as

$$e_{SU} = \delta_\Theta \, \Delta e \, F_{ACT}, \tag{12}$$

where we define an "incubation" function δ_Θ, which is a function of s, V_{ref}, and i (as $(\Theta)_{\text{TOT}}$), and that turns to 1 if at s $(\Theta)_{\text{TOT}} > (\Theta)_{\text{thr}}$, being 0 elsewhere. The incubation function allows the computation of the time instant when the erosion (viz., the removal of material from the target surface) starts in the general case of variable impact conditions. It is now possible to transform the impact pattern into erosion pattern.

We can now obtain the final erosion displacement on the section airfoil line e_{TOT} per unit blade span by summing the scaled contribution for each reference velocity FAST simulation at each pseudo[†]-time step as

$$e_{TOT}(s) = \sum_{V_{ref}=V_{cut-in}}^{V_{cut-out}} \sum_{i=1}^{N_{t\ steps}} e_{SU}^{(V_{ref},i)}(s), \tag{13}$$

where s is the curvilinear abscissa along the blade section profile and $e_{SU}^{(V_{ref},i)}$ is the scaled erosion displacement evaluated for the aerodynamic condition (relative Reynolds number and angle of attack) of the FAST simulation for the reference velocity V_{ref}, and at the time step i.

5 | RESULTS AND DISCUSSION

The machine learnt predictor is now capable of predicting the particle impact pattern and velocity per unit of time at any given aerodynamic condition in which the airfoil is working. Here, we apply the predictor together with FAST[60] and the rain erosion model defined in Section 4 to make an estimation of the annual damage pattern under given wind and rain conditions. The detailed rationale used to evaluate the erosion damage is shown in Figure 11.

As reference, we use the NREL 5-MW wind turbine,[59] manufactured from thermoplastic material and installed in a hypothetic onshore site in which we assume a Weibull shape factor $k = 2$ and scale factor $c = 6.5$. For this sample application, we assume the same rain defined in Castorrini et al.,[39] where we considered an annual rainfall of 2000 mm and an average droplet size of 1 mm.

Here, we report firstly some plots to describe the data used for the computation. Figure 12 shows the Weibull probability density function of the wind velocity during a year and the turbine power-curve, obtained averaging the simulation data with turbulent inflow.

From the wind turbine power curve, we know that the possible inflow wind goes from a cut-in of 3.5 m/s to a cutout of 25 m/s. We created an array of reference velocities at the wind turbine hub, going from 4 to 21 m/s ([‡]) with a step of 1 m/s. For each reference velocity, the TurbSim preprocessing tool[61] is used to generate 650 s of turbulent inflow using the IEC Kaimal Normal turbulence model (see IEC61400-1 standard).

We performed a FAST[60] simulation of the wind turbine for all the selected velocities. For all these simulations (characteristics and description reported in Table 4), we can now extract the time history of the relative Reynolds number and angle of attack at the sample section located at $r = 0.75R$, for the last 600 s (see Figure 13).

Figure 13 reports the variation of the angle of attack and Reynolds number at the sample section in the range of average wind conditions through a waterfall plot. The y axis of the plots is chosen as time step count for each simulation, because the equivalent time associated to each time step depends on the local scale factor. We can observe that both the ranges of angle of attack and Reynolds number fall inside the bounds of the database used to train the impact pattern prediction tool.

The data of particles, site wind, and materials used for the computation are reported in Table 5. We assume the same material for all the points of the analyzed section.

The following calculation allows us to give an estimation of the rain erosion damage after one year of operation in the selected site. The computation of the algorithm of Figure 11 took 14 h to run on a 4-core laptop machine. The final estimation of the damage at the chosen section after 1 year of operation is shown in Figure 14. As explained in the previous sections, this result considers the annual rain flow and wind statistics in the selected site and also the dynamic variability of the relative aerodynamic flow at the section due to the turbulent nature of the wind.

The erosion pattern obtained in the computation is in good agreement with field observations[8,62–64] in which a damage depth ranging in 0.1–1.2 mm was found in machines with 5 years of operations. As it has been noted in field observations, the damage is usually contained in the first 3% portion of the airfoil chord (from LE), mostly on the pressure side, with almost normal distribution around the maximum (see Sareen et al.[8]). We also notice that the erosion plot has a drop in a very narrow neighborhood of the stagnation point. This effect has been already observed in former computations,[36–39] and it is related to the local impact angle of the particles deviated by the aerodynamic flow in this area. The shape and values are also in line with our former computations in Castorrini et al.,[39] which represent an expected average operating condition of the same section. Moreover, this result can be also used as a verification of those former computations.

Figures 15 and 16 show, respectively, the accumulated impact energy and the incubation energy as a function of the airfoil abscissa. The comparison between these two curves gives an indication of the position of the airfoil erosion and of the "safe" regions. The values reported in Figure 16 have been recorded at the moment of local activation of the erosion, thus when the accumulated energy exceeded the incubation energy at the generic point s.

[†]After the scale up procedure, the data corresponding to the time step of the FAST simulation become referred to an extrapolated (extended) time period, by mean of the factor $\frac{T_R}{T_{SIM}} f(V_{ref})$ contained in F_{ACT}

[‡]We avoid some computational cost by not considering the highest velocities, which have very low probability as for the selected Weibull function (Figure 12)

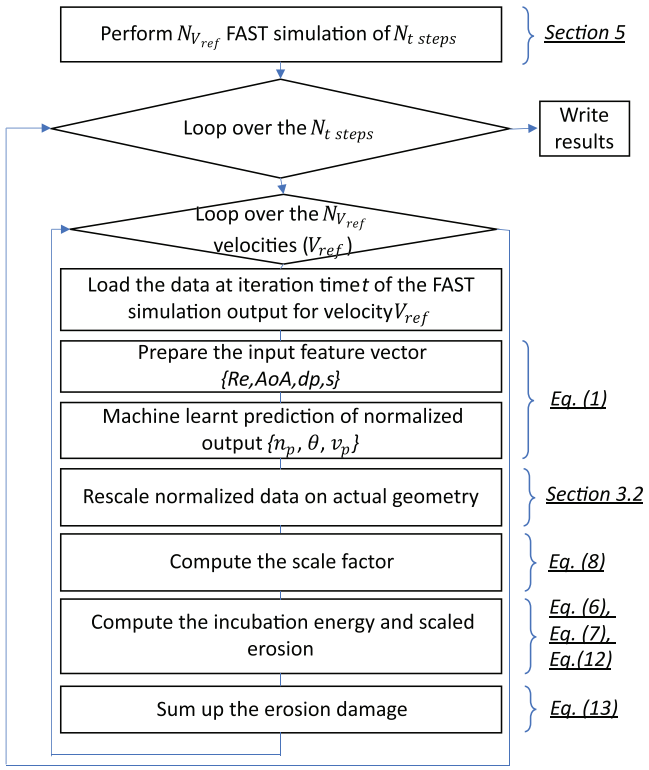

FIGURE 11 Rationale of the algorithm for the computation of the erosion damage

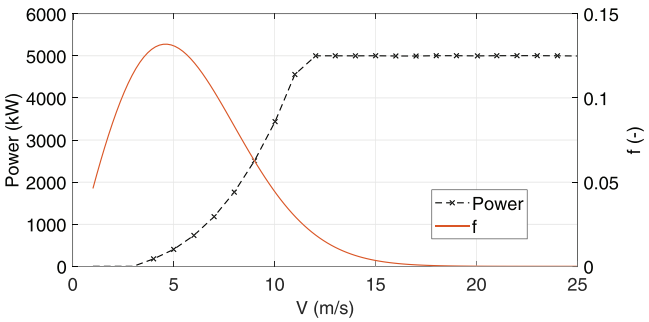

FIGURE 12 Site and machine: Weibull wind distribution in a year *f* (orange) and turbine power curve (black)

TABLE 4 FAST simulations set-up

dt	**0.01 s**
Active computing modules	Elasticity, inflow, aerodynamics, and control
Inflow	Kaimal IEC61400-ed3 NTM (normal turbulence model)
Control	User-defined from bladed-style DLL for variable pitch and velocity

If we look at Figures 7, 8, and 14–16 together, we can observe that all the variables considered in this study are mutually involved in the process of rain erosion of a given blade section in operation. From Figures 7 and 8, we know that, depending on the geometry, relative flow field, and particle sizes, there are areas of the airfoil where it is more probable to have impacts with certain velocity and angle. From the erosion models, we know that the erosion and the incubation energy depend on these features. This is directly observable by the plot in Figure 16, where the regions with lower recorded incubation energy are the regions more prone to have damages. This must be seen in relation also with Figure 15, where the accumulated energy shows, for this application, where the rain flow has stronger effect over the blade section surface. In the end, the intersection of these two plots (Figures 15 and 16) defines the areas where the rain erosion can occur for the given application, while Figure 14 gives the magnitude of the damage.

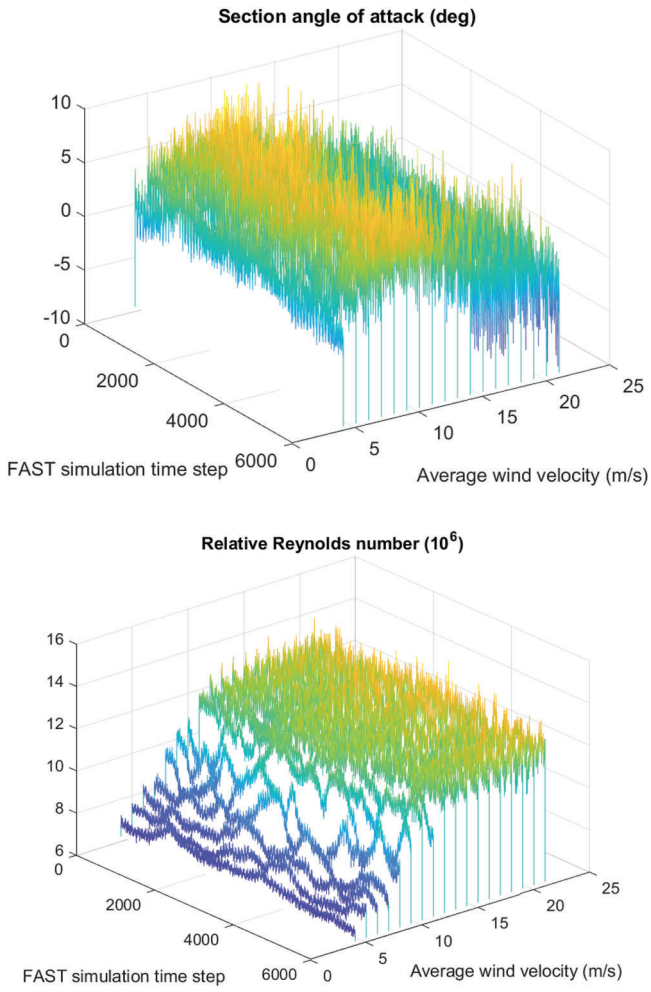

FIGURE 13 Computed section aerodynamics in the FAST simulations: angle of attack (top) and relative Reynolds number (bottom) as functions of FAST simulations time steps and average wind velocity

TABLE 5 Quantities used for the erosion computation

Input	Value
n_{TOT}	6100 m^{-2}
Weibull shape factor k	2
Weibull scale factor c	6.5 m/s
HRF	2 m
d_p	1 mm
Section chord	3.01 m
Speed of sound in liquid	1450 m/s
Speed of sound in coating material	2500 m/s
Coating material density	1600 kg/m^3
Coating material ultimate stress	150 MPa
Coating material fatigue knee	6

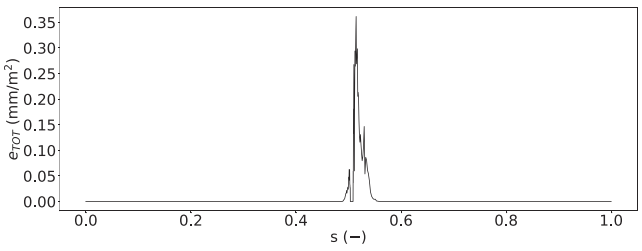

FIGURE 14 Predicted erosion damage after 1 year of operation in terms of erosion displacement per unit of blade span and chord length

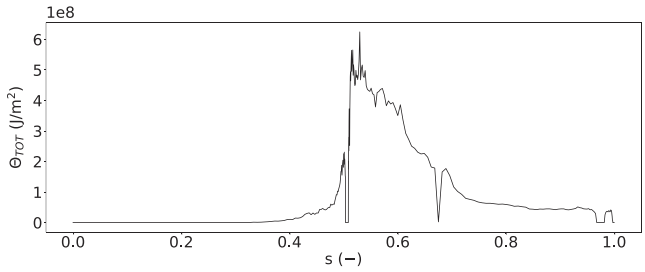

FIGURE 15 Predicted accumulated impact energy per unit of blade span and chord length on the section after 1 year of operation

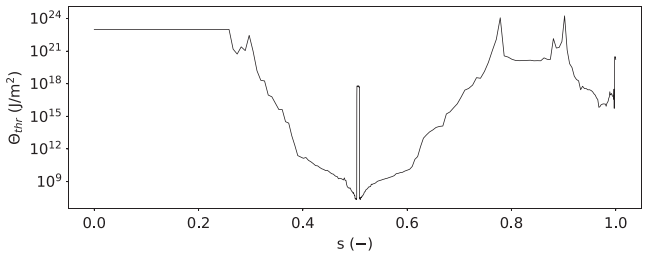

FIGURE 16 Predicted incubation energy needed to activate the erosion

6 | CONCLUSION

In this research paper, we presented a method for the computational prediction of the wind turbine blade erosion, coupling computational particle-fluid dynamics methods with ML, and standard tools for the simulation and certification of wind turbines.

The paper is divided in two main parts: (i) the definition of a ML-aided approach to predict the impact pattern and impact dynamics on an airfoil section, for a given relative wind and particle flow; and (ii) the definition and application of a methodology to couple the resulting tool with the NREL-FAST and a rain erosion model. The final aim of the method is the prediction of rain erosion damage at a given blade section considering the wind turbine in operation for a given period and on a given site of installation.

In order to train the ML regressor, we created a database of cases to correlate a set of features describing the normalized impact pattern and impact dynamics with the features describing the relative freestream wind and particle inflow. The database is then generated with an automatic algorithm that interfaces CFD and particle tracking simulations. Using XGBoost library as ML tool, we obtained accurate predictions of the output features in cross-validation and forwarding tests.

In the second part of the paper, we defined the method to couple the regression tool with FAST and a modified version of the Springer's erosion model. The method integrates and scales-up the erosion damage using the statistics of the wind, the annual rain flow, and the turbulent characteristics of the wind (as prescribed by the IEC61400 standard and processed with the NREL's TurbSim solver). Furthermore, it takes into account all the dynamic and aeroelastic effects related to the turbine in operation, through the simulation of the full turbine performed with FAST.

The final algorithm is applied to predict the rain erosion on an outboard section of the 5-MW NREL wind turbine blade, after 1 year of operation in a site with given annual rain flow and Weibull distribution of the wind velocity. The resulted damage shape and depth agrees with field observations on damaged blade.

However, the main result of this work, in our opinion, is the proposed (and achieved) paradigm shift: no more simulations of a blade specific operating conditions (to be repeated for other conditions), but simulations of all the possible operating conditions of that blade to build a database; then the ML algorithm allows to perform analyses and predictions on any specific operating condition without having to repeat the simulations. Such a predictive tool is very flexible (new database elements can be added at any time), and powerful, allowing to reduce the calculation times (but not the accuracy) of the individual simulations, once the database has been built.

Moreover, it is worth emphasizing that the application of this method to the sections of a blade taken at different radii allows to have a quasi-3-D description of the damaged blade. This could be a strong starting point for optimizing the blade shape in order to reduce the risk of erosion in a given installation site and hence tailoring the blade according to the average weather conditions. Besides, the proposed method can be easily extended to other erosion agents (such as sand or hailstone) by changing the erosion model, and it can be applied also to particle deposition problems.

Finally, we want to remark that this methodology applies in general to any wind turbine aerodynamic section. Accordingly, the method can be easily applied also in the case of vertical axis wind turbines by adopting the proper blade element-based simulation tool.

ACKNOWLEDGMENTS

The authors acknowledge the European Union and the Italian Ministry of Research for financial support under the Programma Operativo Nazionale *Ricerca e Innovazione* 2014–2020. Part of the work has been also supported by Sapienza University of Rome "Progetti Grandi 2019" Grant no. RG11916B8827EABA.

PEER REVIEW

The peer review history for this article is available at https://publons.com/publon/10.1002/we.2609.

ORCID

Alessio Castorrini https://orcid.org/0000-0003-1765-5786

REFERENCES

1. International Renewable Energy Agency. *Future of wind: deployment, investment, technology, grid integration and socio-economic aspects, in: A global Energy transformation paper*; 2019.
2. Enevoldsen P, Xydis G. Examining the trends of 35 years growth of key wind turbine components. *Energy Sustain Dev*. 2019;50:18-26.
3. Molina MG, Mercado PE. Modelling and control design of pitch-controlled variable speed wind turbines. In: Al-Bahadly IH, ed. *Wind turbines*. IntechOpen; 2016.
4. Igwemeziea V, Mehmanparasta A, Kolios A. Current trend in offshore wind energy sector and material requirements for fatigue resistance improvement in large wind turbine support structures—a review. *Renew Sustain Energy Rev*. 2019;101:181-196.
5. Enevoldsen P, Valentineb SV, Sovacoola BK. Insights into wind sites: critically assessing the innovation, cost, and performance dynamics of global wind energy development. *Energy Policy*. 2018;120:1-7.
6. Dalili N, Edrisy A, Carriveau R. A review of surface engineering issues critical to wind turbine performance. *Renew Sustain Energy Rev*. 2009;13(2):428-438.
7. Wood K. Blade repair: closing the maintenance gap. *Compos Technol*. 2011;9(2).
8. Sareen A, Sapre CA, Selig MS. Effects of leading edge erosion on wind turbine blade performance. *Wind Energy*. 2014;17(10):1531-1542.
9. Keegan MH, Nash DH, Stack MM. On erosion issues associated with the leading edge of wind turbine blades. *J Phys D Appl Phys*. 2013;46(38):383001.
10. 3M, 2011, A 3M study is the first to show the effects of erosion on wind turbine efficiency, www.pressebox.com
11. Sierra AH, Pérez EG. *Wind farm owner's view on rotor blades—from O&M to design requirements, International Conference on Wind Turbine Rotor*. Bremen, Germany: BladeO&M; 2013.
12. Rempel L. Rotor blade leading edge erosion-real life experience, Wind Systems Magazine; 2012.
13. Mishnaevsky L Jr. Toolbox for optimizing anti-erosion protective coatings of wind turbine blades: overview of mechanisms and technical solutions. *Wind Energy*. 2019;22(11):1636-1653.
14. Zhang S, Dam-Johansen K, Bernad PL Jr, Kiil S. Rain erosion of wind turbine blade coatings using discrete water jets: effects of water cushioning, substrate geometry, impact distance, and coating properties. *Wear*. 2015;328-329:140-148.
15. Amirzadeh B, Louhghalam A, Raessi M, Tootkaboni M. A computational framework for the analysis of rain-induced erosion in wind turbine blades, Part I: stochastic rain texture model and drop impact simulations. *J Wind Eng Ind*. 2017;163:33-43.
16. Amirzadeh B, Louhghalam A, Raessi M, Tootkaboni M. A computational framework for the analysis of rain-induced erosion in wind turbine blades, Part II: drop impact-induced stresses and blade coating fatigue life. *J Wind Eng Ind*. 163:44-54.
17. Slot HM, Gelinck ERM, Rentrop C, van der Heide E. Leading edge erosion of coated wind turbine blades: review of coating life models. *Renew Energy*. 2015;80:837-848.
18. Eisenberg D, St. Laustsen JS. Wind turbine blade coating leading edge rain erosion model: development and validation. *Wind Energy*. 2018;21(10):942-951.
19. Li D, Zhao Z, Li Y, Wang Q, Li R, Li Y. Effects of the particle Stokes number on wind turbine airfoil erosion. *Appl Math Mech*. 2018;39(5):639-652.
20. Maniaci DC, White EB, Wilcox B, Langel CM, van Dam CP, Paquette JA. Experimental measurement and CFD model development of thick wind turbine airfoils with leading edge erosion. *J Phys: Conf Ser*. 2016;753:022013.
21. Hossam El-Din A, Diab A, Ghoneim Z. Assessment of losses in annual energy production of wind turbines subjected to sand erosion, Twelfth International Conference of Fluid Dynamics, 19–20 December, Cairo, Egypt; 2016.
22. Fiore G, Selig MS. A simulation of operational damage for wind turbine blades, 32nd AIAA Applied Aerodynamics Conference, Atlanta, GA. 2014
23. Fiore G, Fujiwara GEC, Selig MS. A damage assessment for wind turbine blades from heavy atmospheric particles, 53rd AIAA Aerospace Sciences Meeting, Kissimmee, Florida; 2015.
24. Fiore G, Selig MS. Simulation of damage progression on wind turbine blades subject to particle erosion, 54th AIAA Aerospace Sciences Meeting, San Diego, California; 2016.
25. Borello D, Rispoli F, Venturini P. An integrated particle-tracking impact/adhesion model for the prediction of fouling in a subsonic compressor. *J Eng Gas Turb Power*. 2012;134(9):092002.
26. Borello D, Anielli D, Rispoli F, Salvagni A, Venturini P. Unsteady CFD analysis of erosion mechanism in the coolant channels of a rotating gas turbine blade, ASME Turbo Expo, June 15–19, 2015, Montreal, Canada.
27. Borello D, Capobianchi P, De Petris M, Rispoli F, Venturini P. Unsteady RANS analysis of particles deposition in the coolant channel of a gas turbine blade using a non-linear model, ASME Turbo Expo 2014, Dusseldorf, Germany, paper no. GT2014–26252.
28. Agati G, Borello D, Rispoli F, Venturini P. An innovative approach to model temperature influence on particle deposition in gas turbines, Turbo Expo 2016, Seoul, South Korea, 13–17 June, 2016, paper no. GT2016-57997.
29. Corsini A, Marchegiani A, Rispoli F, Venturini P, Sheard AG. Predicting blade leading edge erosion in an axial induced draft fan, ASME transactions. *J Eng Gas Turb Power* (ISSN:0742–4795). 2012;134(4):042601. https://doi.org/10.1115/1.4004724

30. Corsini A, Rispoli F, Venturini P, Sheard G. Numerical simulation of coal-fly ash erosion in an induced draft fan. *ASME J Fluid Eng*. 2013;135:1-12. https://doi.org/10.1115/1.4024127
31. Cardillo L, Corsini A, Borello D, Delibra G, Salvagni A, Rispoli F, Venturini P. Modelling of particle transport, erosion and deposition in power plant gas paths, Turbo Expo 2016, Seul, South Korea, 13–17 June, 2016, paper no. GT2016–57984.
32. Cardillo L, Corsini A, Delibra G, Rispoli F, Sheard AG, Venturini P. Simulation of particle-laden flows in a large centrifugal fan for erosion prediction, ASME Turbo Expo 2014, Dusseldorf, Germany, paper no. GT2014–25865.
33. Corsini A, Castorrini A, Morei E, Rispoli F, Sciulli F, Venturini P. Modeling of rain drop erosion in a multi-MW wind turbine, ASME Turbo Expo, June 15–19, 2015, Montreal, Canada (paper GT2015–42174).
34. Castorrini A, Corsini A, Rispoli F, Venturini P, Takizawa K, Tezduyar TE. In: Bazilevs Y, Takizawa K, eds. *SUPG/PSPG computational analysis of rain erosion in wind-turbine blades. In: Advances in computational fluid-structure interaction and flow simulation*. Springer; 2016.
35. Baxter LL, Smith PJ. Turbulent dispersion of particles: the STP model. *Energy Fuel*. 1993;7(6):852-859.
36. Castorrini A, Corsini A, Morabito F, Rispoli F, Venturini P. Numerical simulation with adaptive boundary method for predicting time evolution of erosion processes, Turbo Expo 2017, Charlotte, North Carolina, 26–30 June, 2017, paper no. GT2017-64675.
37. Castorrini A, Corsini A, Rispoli F, Venturini P. Numerical simulation of the blade aging process in an induced draft fan due to long time exposition to fly ash particles, Turbo Expo 2018, June 11–15, 2018, Oslo, Norway, paper no. GT2018-76740.
38. Castorrini A, Corsini A, Rispoli F, Venturini P, Takizawa K, Tezduyar TE. Computational analysis of wind-turbine blade rain erosion. *Comput Fluids*. 2016;141:175-183.
39. Castorrini A, Corsini A, Rispoli F, Venturini P, Takizawa K, Tezduyar TE. Computational analysis of performance deterioration of a wind turbine blade strip subjected to environmental erosion. *Comput Mech*. 2019;64(4):1133-1153.
40. Stein K, Tezduyar TE, Benney R. Automatic mesh update with the solid-extension mesh moving technique. *Comput Methods Appl Mech Eng*. 2004;193(21–22):2019-2032.
41. Castorrini A, Venturini P, Corsini A, Rispoli F. Simulation of the deposit evolution on a fan blade for tunnel ventilation. *J Eng Gas Turb Power*. 2020;142(4):041010. https://doi.org/10.1115/1.4044930
42. Castorrini A, Venturini P, Corsini A, Rispoli F, Takizawa K, Tezduyar TE. Computational analysis of particle-laden-airflow erosion and experimental verification. *Comput Mech*. 2020;65(6):1549-1565. https://doi.org/10.1007/s00466-020-01834-0
43. Sommerfeld M, van Wachem B, Oliemans R. Best practice guidelines. ERCOFTAC Special Interest Group on "Dispersed turbulent multi-phase flow", 2008.
44. Crowe CT, Mechaelides EE. Basic concepts and definitions. In: Crowe CT, ed. *Multiphase flow handbook*. Taylor & Francis: Boca Raton; 2006.
45. Grant G, Tabakoff W. Erosion prediction in turbomachinery resulting from environmental particles. *J Aircr*. 1975;12(5):471-478.
46. Tabakoff W, Kotwal R, Hamed A. Erosion study of different materials affected by coal ash particles. *Wear*. 1979;52(1):161-173.
47. Hutchings IM, Winter RE. Particle erosion of ductile metals: a mechanism of material removal. *Wear*. 1974;27(1):121-128.
48. Springer GS, Yang CI, Larsen PS. Analysis of rain erosion of coated materials. *J Compos Mater*. 1974;8(3):229-252.
49. Andreoli M, Gabriele S, Venturini P, Borello D. New model to predict water droplets erosion based on erosion test curves. Application to on-line water washing of a compressor, Turbo Expo 2019, June 17–21, 2019, Phoenix, Arizona, paper no. GT2019–92033.
50. Venturini P, Andreoli M, Borello D, Rispoli F, Gabriele S. Modelling of water droplets erosion on a subsonic compressor cascade. *Flow Turbul Combust*. 2019;103(4):1109-1125.
51. Armenio V, Fiorotto V. The importance of the forces acting on particles in turbulent flows. *Phys Fluids*. 2001;13(8):2437-2440.
52. Greifzu F, Kratzsch C, Forgber T, Lindner F, Schwarze R. Assessment of particle-tracking models for dispersed particle-laden flows implemented in OpenFOAM and ANSYS FLUENT. *Eng Appl Comput Fluid Mech*. 1997;10(1):30-43.
53. Chen T, Guestrin C. Xgboost: A scalable tree boosting system. In *Proceedings of the 22nd acm sigkdd international conference on knowledge discovery and data mining*. 2016;785–794.
54. Chen T, He T, Benesty M, Khotilovich V, Tang Y. Xgboost: extreme gradient boosting. *R package version 0.4–2*, 1–4. 2015
55. Fan J, Wang X, Wu L, et al. Comparison of support vector machine and extreme gradient boosting for predicting daily global solar radiation using temperature and precipitation in humid subtropical climates: a case study in China. *Energ Conver Manage*. 2018;164:102-111.
56. Saigo H, Nowozin S, Kadowaki T, Kudo T, Tsuda K. gBoost: a mathematical programming approach to graph classification and regression. *Mach Lear*. 2009;75(1):69-89.
57. https://github.com/dmlc/xgboost
58. Bergstra J, Bengio Y. Random search for hyper-parameter optimization. *J Mach Learn Res*. 2012;13:281-305.
59. Jonkman J, Butterfield S, Musial W, Scott G. *Definition of a 5-MW reference wind turbine for offshore system development* (No. NREL/TP-500-38060). National Renewable Energy Lab.(NREL), Golden, CO (United States). 2009
60. Jonkman JM, Buhl ML Jr. *FAST user's guide*. 365 Golden, CO: *National Renewable Energy* Laboratory; 2005:366.
61. Jonkman BJ, Buhl ML Jr. *TurbSim user's guide (No. NREL/TP-500-39797)*. Golden CO (United States): National Renewable Energy Lab.(NREL); 2006.
62. 3M, A 3M study is the first to show the effects of erosion on wind turbine efficiency, 2011, https://www.pressebox.com/pressrelease/3m-deutschland-gmbh/a-3m-study-is-the-first-to-show-the-effects-of-erosion-on-wind-turbine-efficiency/boxid/445007. Accessed on 28 February 2020.
63. Han W, Kim J, Kim B. Effects of contamination and erosion at the leading edge of blade tip airfoils on the annual energy production of wind turbines. *Renew Energy*. 2018;115:817-823.
64. Gaudern D. A practical study of the aerodynamic impact of wind turbine blade leading edge erosion. *J Phys: Conf Ser*. 2014;524:012031.

How to cite this article: Castorrini A, Venturini P, Corsini A, Rispoli F. Machine learnt prediction method for rain erosion damage on wind turbine blades. *Wind Energy*. 2021;1–18. https://doi.org/10.1002/we.2609